Energy-based ductile failure predictions in cracked friction-stir welded joints

H.R. Majidi [a], A.R. Torabi [b], M. Zabihi [a], S.M.J. Razavi [c], F. Berto [c*]

[a] *Department of Mechanical Engineering, Iran University of Science and Technology, Narmak, 16846 Tehran, Iran*

[b] *Fracture Research Laboratory, Faculty of New Sciences and Technologies, University of Tehran, Tehran, Iran*

[c] *Department of Mechanical and Industrial Engineering, Norwegian University of Science and Technology (NTNU), Richard Birkelands vei 2b, 7491, Trondheim, Norway.*

Abstract

This research aims to study the fracture behaviour in dissimilar aluminum alloys adjoined by friction stir welding (FSW). In this way, experimental data dealing with this topic was taken from the recent literature. In those experimental results, two metal sheets made of Al 7075-T6 and Al 6061-T6 were adjoined together by FSW in the form of well-known specimen, namely the cracked semi-circular bend (CSCB) and then they are tested under mixed mode I/II loading condition. Due to the fact that substantial plastic behavior exist in the welded material and consequently significant plastic deformations were observed around the crack tip, failure prediction of the mentioned specimens needs failure prediction models in the basis of the elastic-plastic fracture mechanics which can be realized as sophisticated operations inquiring long time. In this way, the Equivalent Material Concept (EMC) is utilized in this research and then coupled with two eligible energy-based criteria, namely the averaged strain energy density (ASED) and J-integral criteria. Thus, the critical failure load of the welded samples is predicted. Comparison between the empirical data and theoretical predictions from energy-based evaluations showed that this model has enough capability in estimating the critical failure load of the CSCB samples.

* Corresponding author (F. Berto), E-mail: filippo.berto@ntnu.no

Keywords: Ductile failure; Friction stir welding (FSW); Equivalent Material Concept (EMC); averaged strain energy density (ASED); J-integral

1. Introduction

Aluminum alloys have been so applications among modern industries including lightweight cars and trains, fuselage of aerospace structures, ships deck and body since they possess desired characteristics including low weight, high strength, high resistance in corrosion factor, etc. Due to outstanding progress in joining various grades and series of aluminum alloys by the FSW technique in the past two decades or so, one of the most challenging issues concerning the welding process of these alloys, which has been the inability of the conventional fusion welding methods to be effective on some particular series categorized as non-weldables, has been eliminated. Hence, many researchers have conducted numerous studies in order to determine the performance of physical and mechanical factors in FSW weldments. Various aspects of characteristics in FSWed Al-Al joints for two conditions of similar and dissimilar joints were investigated, indeed. Among these features are some well-known ones, including tensile and flexural strengths, wear and corrosion resistance, microstructures and impact strength. For instance the efficacy of input parameters on the mechanical characteristics in AA5083-H111 joint were conducted by Kasman and Kahraman [1]. In another research, the pin profile and pin rotational speed effects (i.e. welding tools) on the AA7075-T6 joint's microstructure, microhardness, tensile strength and elongation via FSW technique were studied by Bahemmat et al. [2]. In some researches, the optimization of the FSW process in aluminum alloys concerning various aspects including tailor welding [3], minimizing the residual stress [4] and so on, was the main topic. Another specific ability that the FSW technique provides and is vastly popular in numerous high-tech productions; in this way, it can be refered to huge industries like train, car, aerospace, and ship structures is dissimilar joining of

aluminum alloys. For instance, in order to study the influence of input ingredients of FSW on the mechanical charachteristics of dissimilar aluminum welded joints, some researchers [5-7] have fabricated the bi-metal joints in their researches, respectively. The optimization of the process parameters in a dissimilar Al-Al (5xxx and 6xxx series) welded joint via the FSW was done by Aliha et al. [8]. They acquired the artificial neural network method in order to optimize both the microhardness and tensile strength of the butt joint at the same time in a multi-objective manner. Although promissing ultimate strength and hardness can be obtained by FSWing, however the other mechanical features and integrity indices should endure the applied service loads in practice as well. For example, crack propagation as result of fatigue loads, excessive forces and impact can possibly be considered as the failure modes for FSW-manufactured parts and structures; hence it is vital to assess the fracture toughness of material facing the initiation of the crack or propagation concerning the reliable use and the integrity evaluation of FSWed parts in practical applications. Also some published papers were conducted on determination of the crack growth resistance and fracture toughness FSW joints. For instance, the propagation fatigue crack characteristic of AA6082-T6 alloy which has been butt-welded by the FSW technique utilizing edge cracked compact tension specimen (CT) testing in the condition of mode I loading was investigated by Moreira et al. [9]. In their study, the fatigue crack growth curves were acquired for various weldment locations such as stir zone (SZ), heat affected zone (HAZ) and base material (BM) areas. It was resulted that the crack propagation rate in the SZ area is lower compared to the BM and HAZ areas. Additionally, Raghuram [10] conducted a research on fatigue crack growth response in new aluminum alloys generations including Al2195 and Al2219 that are being utilized in new super lightweight space shuttles for manufacturing the external tank of them. He produced dissimilar AA2195-AA2214 butt joints by FSW and then investigated the factors of some parameters on the weldments fatigue life including stress ratio, periodic overloading and corrosion preventive compound. In that study, he utilized a rectangular beam with a central drilled hole in the

weld area, containing two pre-cracks which were extruded from the cavity along the weld path, while facing a far-field tension. Mokhtar et al. [11] studied the propagation of fatigue crack in a welded AA6061 plate with 10 mm thickness by employing the CT geometry of their tests according to ASTM-E399 and E647 standards. In the meantime, they fixed some input parameters like the rotational and transverse speeds, alongside the tool's size and the geometry. As opposed to that research, Alavinia and Shirazi [12] conducted a study on investigating the tool's rotational and linear speeds influence on fracture toughness and fatigue life of some FSW-welded copper sheets. In the research conducted by Alavinia and Shirazi, some compact tension (CT) specimens of various weld zone locations were cut and tested, leading to the conclusion that compared to the base metal, the rate of fatigue crack growth in HAZ is noticeably higher because of the heat transfer occurrence to plunging section. It is worth mentioning that both the realignment and the dynamic recrystallization of grains within SZ can improve the resistance against the fatigue crack growth. Ghahremani Moghadam and Farhangdoost [13] investigated the pin's transverse and rotational speeds effect on the fracture characteristics of AA2024-T351 alloy utilizing chevron notched CT sample. It was illustrated in the study that the rate of fatigue crack growth is affected by the tool speed. As a matter of fact, the LCC and fracture toughness of tested samples have been reduced by up to 50%. This is basically due to the fact that at higher tool speeds, the defect initiation in the FSW area is more probable, consequently leading to the fracture resistance reduction in the samples. In another research, the fracture resistance of FSWed and metal inert gas welded joints out of AlCu4SiMg were investigated by Kulekci et al. [14]. They evaluated the values of the fracture toughness for the welded joints by using empirical data evaluated from Vickers hardness and Charpy impact experiments. They concluded that the values of fracture toughness for their tested FSWed joints are remarkably higher than those of them manufactured by the conventional fusion welding approach. This phenomenon has been accured owing to existing the lower heat input and lack of melting and filler metal in the FSW approach.

Seib et al. [15] has evaluated the residual strength and fracture toughness of materials utilized for aerospace structures by testing a welded sample containing a center crack by FSW technique. In several dissimilar AA5083-AA6061 alloys adjoined by the FSW technique, the fracture toughness have been measured by Syafiq et al. [16] with different input parameters. Aliha et al. [17] have investigated the interface notch fracture strength by considering the results of input parameters of FSW in several bi-material samples manufactured by Al5083/Cu weldment. Albeit, in instances with industrial applications, the cracks in FSWed specimens may germinate and growth under multi-axial loading conditions. Especially, a mixed mode I/II fracture can probably harness the overall failure in cracked components manufactured by FSW. However, by searching in the literature it can be stated that mixed mode fracture behaviour of such welded joints was scarcely studied in previous researches. In this regard, the fracture toughness of samples welded by FSW have been studied by Sutton et al. [18]. In their experiments, they provided some compact tension shear (CTS) specimens for measuring fracture toughness for different mode mixtures. Before these researches, no theoretical research could be found in the literature dealing with predicting the crack trajectory, and also failure load behavior of FSWed specimens subjected to mixed tensile-shear loadings. Hence, in order to fulfill this gap, a number of fracture experiments in the wide range of mode mixities have been conducted by Torabi et al. [19] on dissimilar aluminum FSWed components by utilizing a well-known speciemen, namely a CSCB sample. In their theoretical part, they have estimated the obtained empirical results of critical failure loads in several cracked samples by using two well-known stress-based criteria, so called EMC-MTS and EMC-MS criteria.

Using EMC in a few researches showed that it has high potentiality for coupling with various fracture prediction models, like ASED [20], MTS [21], MS [21], TCD [22] and J-integral criteria [23], providing new EMC-based failure models for failure behaviour of diverse notched domains having a significant ductile behavior or notched members with nonlinear bahaviour. In this regard, it is tried in

this research to check the potential of two energy-based criteria, namely the EMC-ASED and EMC-J criteria which were frequently assessed in failure prediction of notched ductile members, in prediction of ductile behavior in FSWed CSCB specimens tested by Torabi et al. [19].

2. Experimental procedure and results reported in the literature

As aforementioned, Torabi et al. [19] have worked on experimental research in which several FSWed specimens have been tested in the two conditions of mixed mode I/II and also pure mode I. To achieve this purpose, first, some sheets with dimensions of 200×100×3 mm made of Al 7075-T6 and Al 6061-T6 have been butt welded by applying the FSW technique. The tensile properties of these materials are presented in Table 1. To achieve sound quality and defect free joints, four parameters which have main role in FSW process including tool rotational, the pin shape, the transverse speeds and the offset values have been checked accurately and optimized.

Table 1 Tensile properties of Aluminums utilized for the FSW butt welded joints [19].

Material	Yield strength (MPa)	Ultimate strength (MPa)	Total elongation (%)	Elastic modulus (GPa)
Al 7075-T6	521	583	8	74
Al 6061-T6	276	292	11	67

They have utilized a cracked semi-circular bend (CSCB) in their research for experiments of FSWed joints. The CSCB specimen has been shown schematically in Fig. 1. All dimension parameters of the CSCB sample have been introduced in Fig. 1. Table 2 presents the values of a, R, and $2S$ which were considered constant in all experiments. To find the optimum values of the two parameters, entitled tool transverse and rotational speeds, a trial-and-error procedure has been applied and after conducting this operation, these two values have been obtained equal to 80 mm/min and 1000 rpm, respectively. Also, a fixed pin tilt angle of 3◦ was used for welding of all the tested aluminum joints. The appearance of a

Al-Al sample has been shown in Fig. 2. This figure demonstrates that no surface defect was created in the weld region and it seems that quality of the welded joints is quite promising.

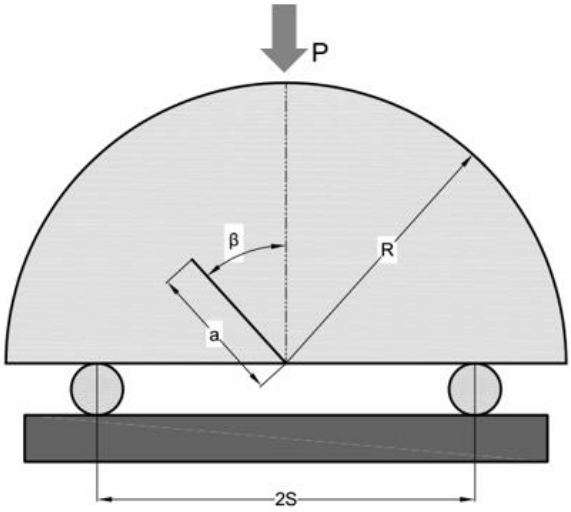

Fig. 1 Schematic of CSCB specimen.

Table 2 Dimensions of CSCB sample.

Radius (*R*)	30 mm
Crack length (*a*)	15 mm
Distance between the two supports (2*S*)	40 mm

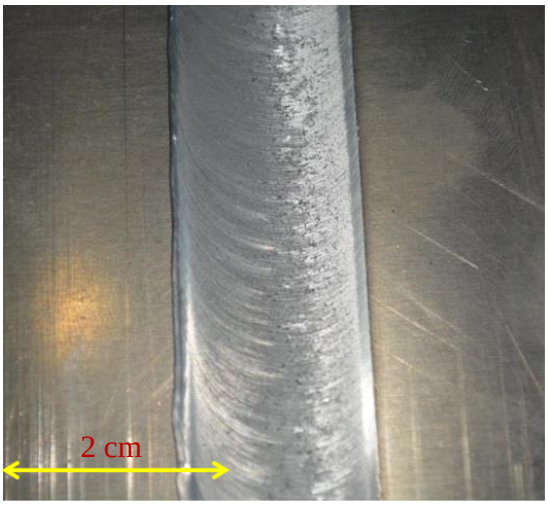

Fig. 2 Surface quality of a sample welded joint.

A water-jet machine has been utilized for producing all CSCB specimens. A very slender edge crack was created by wire-cut machine for each CSCB specimen with tip radius and length of 0.1 mm and 15 mm, respectively. Thus, a CSCB specimen has been provided for experiments. These specimens were tested subjected to conventional three-point bending setup. For conducting pure mode I loading, the CSCB specimen with vertical (i.e. β=0) crack was examined and consequently, for providing mixed mode fracture, the cracked CSCB specimens were tested.

In order to cover various in-plane modes of loading, including pure mode I and mixed mode I/II loadings, the pre-crack inclination angle β was set to 0 for pure mode I loading, and 26, 45, and 56 for mixed mode I/II loading conditions providing a wide range of modes I and II combinations for all CSCB welded samples. A constant loading rate of 1 mm/min with displacement-control conditions has been utilized for all experiments. Each configuration has been repeated three times. The experimental results of critical failure load for the CSCB welded samples are listed in Table 3.

Table 3 list of experimental failure loads for the whole CSCB samples.

β (deg.)	P_1 (N)	P_2 (N)	P_3 (N)	$P_{av.}$ (N)
0	6905	6948	6891	6915
25	9259	10904	8608	9590
45	17552	17538	17023	17371
56	29750	32085	32018	31284

The crack growth for the two arbitrary CSCB joints is shown in Fig. 3. As it can be observed in Fig. 3, the crack tip experienced considerable roundness and opening. In other words, it can be stated that remarkable plastic deformations exist around the crack tip. By observing these experimental results, it can be stated that the failure behaviour of all tested joints show ductile failure.

Moreover, a remarkable nonlinear region before the peak load can be observed in the load-displacement curves of the tested FSWed specimens (for instance see Fig. 4). By observing the large

plastic deformations at the ligament, it can be stated that two types of scale yielding exist in tested CSCB specimens, including LSY or MSY failure regimes. By conducting elastic-plastic FE calculations, it has been shown by them that in pure mode I and prevalent mode II loadings, tested samples have been experienced plastic deformations equal to about 25% and 40% of the ligament at failure instance, respectively.

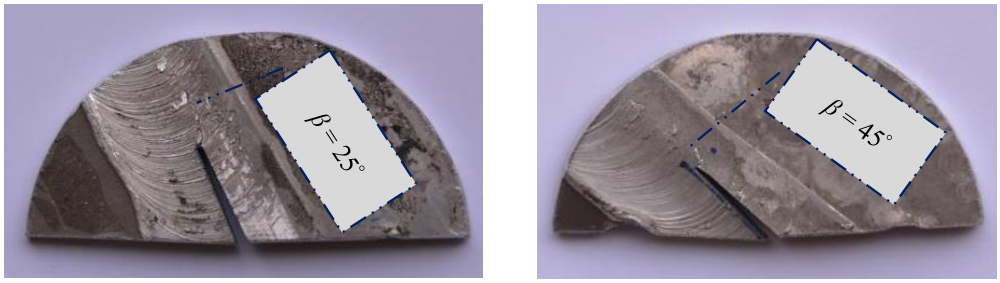

Fig. 3 representative CSCB specimens.

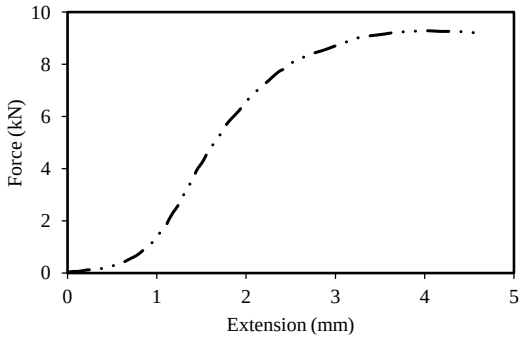

Fig. 4 Representative load-displacement curve related to a specific CSCB component [19].

As mentioned above that the FSWed CSCB samples have ductile behaviour, it can be concluded that to predict the critical failure load of these specimens, ductile failure prediction criteria in the field of elastic-plastic fracture mechanics should be utilized. Hence, Torabi et al. [19] theoretically predicted the failure loads of the CSCB specimens without conducting elastic-plastic analyses by means of two stress-based criteria in combination with the EMC, providing two stress-based criteria with EMC evaluations. However, in this research, it is attempted to check the potential of EMC-ASED and EMC-J

criteria in prediction of ductile behavior in FSWed CSCB specimens reported by Torabi et al. [19]. In further sections, the empirical data of critical failure loads are predicted by using two energy-based failure models as aforementioned.

3. Energy-based criteria based on EMC evaluations

3.1. A brief description of EMC

For the first time, a new theory in the field of fracture mechanics entitled Equivalent Material Concept (EMC) has been presented by Torabi [24]. For example, consider Fig. 5. (a) representing a typical tensile stress-strain curve for a ductile material.

According to EMC, the mechanical behavior of ductile material is formulated with a virtual brittle material having the same elastic modulus, E and the *K*-based fracture toughness, but with an unknown tensile strength (σ_f^*). Fig. 5. (b) illustrates the stress-strain curve of the equivalent brittle material where the gray area identifies the strain energy density until brittle fracture. This area should be assumed to be equal to $\sigma_f^{*2}/2E$. Based on EMC, it can be stated that the gray areas in Figs. 5. (a) and 5. (b) should be equal. Therefore:

$$(SED)_{EMC} = \frac{\sigma_f^{*2}}{2E} \quad \rightarrow \quad \sigma_f^* = \sqrt{2E(SED)_{EMC}} \tag{1}$$

The parameter σ_f^* permits us to couple any brittle fracture criteria with EMC for providing ductile failure predictions. In Ref. [19], the value of $(SED)_{EMC}$ has been reported equal to 14.93 MPa. Thus, by considering E = 70.5GPa and $(SED)_{EMC}$ = 14.93 MPa into Eq. (1), the parameter σ_f^* is obtained to be equal to 1450 MPa.

The EMC has been successfully utilized in many researches to predict the failure capacity in notched ductile members or notched brittle ones with significant non-linear behaviour [25]. In the next section, the ASED and J-integral criteria are explained and by applying the value of σ_f^* in these failure prediction models, the experimental results of failure loads for the tested FSWed components can be theoretically estimated. In the forthcoming, two energy-based criteria are elaborated for predicting the experimental results of the tested FSWed CSCB specimens.

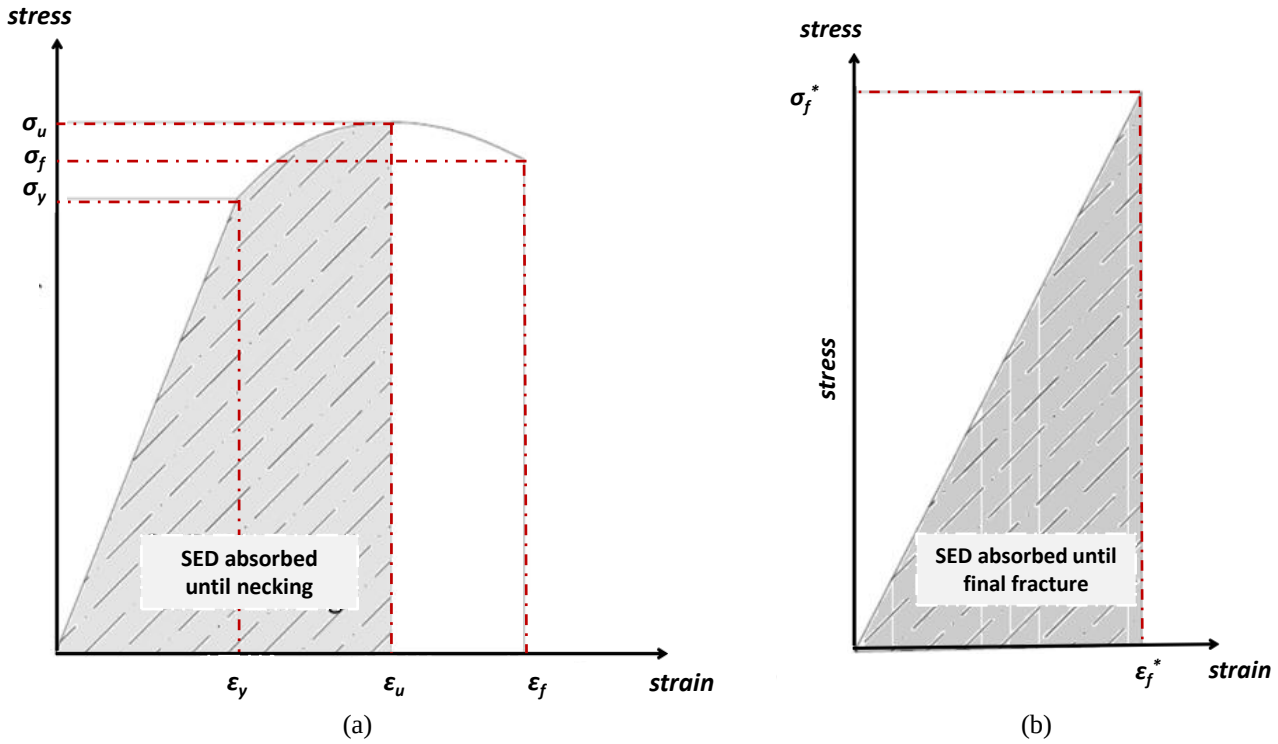

Fig. 5. (a) Typical tensile stress-strain curve for a ductile material (b) SED absorbed by the equivalent material until final fracture.

3.2. EMC-ASED criterion

Lazzarin and Zambardi [26] proposed a volumetric energy-based criterion namely ASED for failure prediction of cracked and notched components under both monotonic and cyclic loadings. According to ASED criterion, when the average value of SED over a cylindrical control volume around the crack tip approaches a critical value, the component containing the crack will fail. Dealing with materials with

linear elastic behavior, the size of control volume is a function of the ultimate tensile strength, σ_u, the fracture toughness, K_c, and the Poisson's ratio, ν of material and for plane-stress condition it can be calculated using [27]

$$R_C = \frac{(5-3\upsilon)}{4\pi}\left(\frac{K_c}{\sigma_u}\right)^2 \tag{2}$$

The critical SED value is a material dependent parameter, which defines the onset of failure in the specimen. For materials with linear elastic behavior, the critical SED depends on the ultimate tensile strength and the fracture toughness K_c and it can be calculated using the following expression [27]

$$W_{cr} = \frac{{\sigma_u}^2}{2E} \tag{3}$$

In order to calculate the failure loads of the cracked components made of ductile materials, one can replace the equivalent ultimate tensile strength with ultimate tensile strength in Eqs. 2 and 3 and obtain the size of control volume and critical SED values using Eqs. 4, and 5.

$$R_{c/EMC} = \frac{(5-3\upsilon)}{4\pi}\left(\frac{K_c}{\sigma_f^*}\right)^2 \tag{4}$$

$$W_{cr/EMC} = \frac{{\sigma_f^*}^2}{2E} \tag{5}$$

By using Eq. (4), the control radius $R_{c/EMC}$ for the welded zone is found as 0.268 mm. The critical SED values, $W_{cr/EMC}$ was equal to 14.91 MJ/m3. The average SED value inside the control volume, $\bar{W}_{EMC}$ was numerically calculated using finite element analysis. Finite element models of pre-cracked CSCB specimens with dimensions given in Table 2 (i.e. the same geometry utilized for the manufactured and tested welded samples) were considered for failure analyses with linear elastic behavior assumption. Linear elastic properties of the tested material (i.e. E = 70.5 GPa and ν = 0.33) were used in the numerical analyses. The 8-node biquadratic plane-stress quadrilateral elements were used to mesh the finite element models under mixed mode loading conditions. As illustrated in Fig. 6, very fine elements

were used in the vicinity of the crack tip to obtain accurate results. However, according to the mesh sensitivity results obtained for average SED values in the control volume, it is clear that the ASED method is not sensitive to element size. This is in accordance with the previous findings reported by Rice [28] (see Table 4).

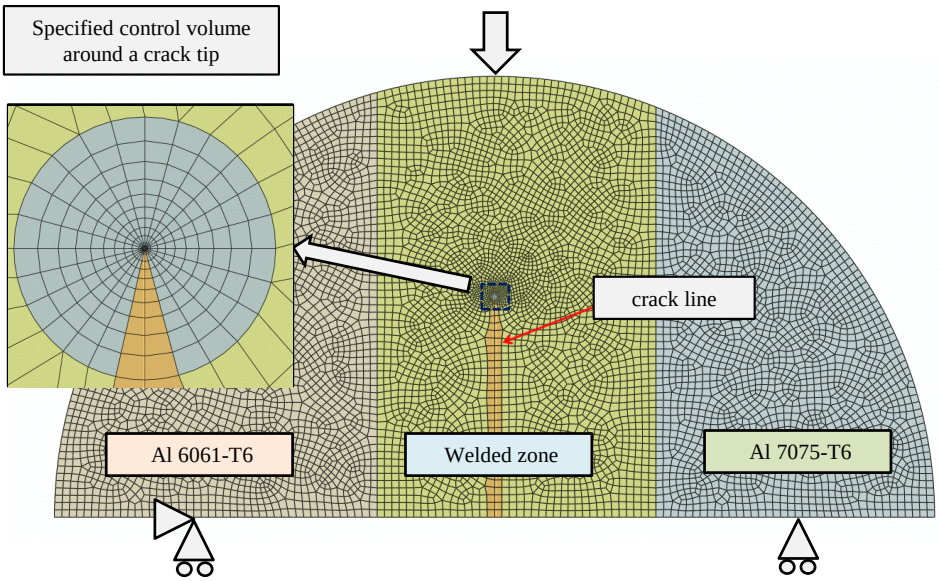

Fig. 6. Typical mesh pattern and boundary condition of CSCB model under pure mode I loading.

Table 4 Mesh sensitivity analysis with different element sizes.

Mesh pattern	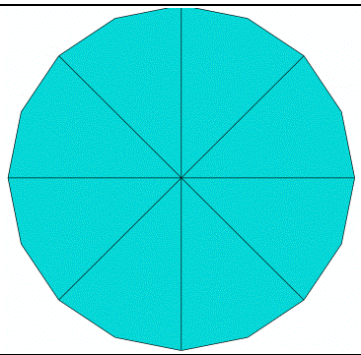	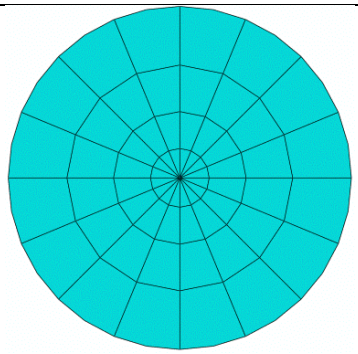	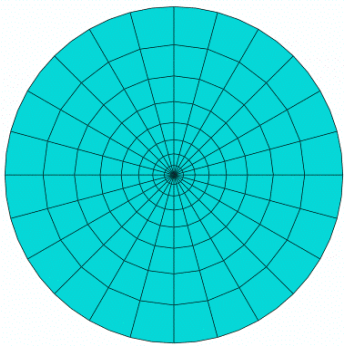
$\bar{W}_{EMC}$	3.24e-07	3.29e-07	3.29e-07

3.3. EMC-J criterion

J-integral is one of the applicable parameter which is usually used to compute the local stress concentration fields around cracks and notches and also to predict the propagation process of cracks in

various cracked and notched members. Cherepanov [29] has proposed for the first time the J-integral and after his proposal, Rice [28] has independently extended previous proposal. Rice has introduced a new contour path integral independent of the path around the crack tip, so called J-integral. Thereafter, Kim et al. [30] and Chen and Lu [31] utilized J-integral concept for estimating the fracture behaviour of any cracked and notched components, respectively.

The J-integral can generally be computed by using the following expression [29]:

$$J_k = \oint_{\varphi} \left(W n_k - T_i \frac{\partial u_i}{\partial x_k} ds \right) \ (k = 1\ ,2) \tag{6}$$

The J-integral can be directly related to the fracture toughness for isotropic and perfectly brittle materials. It is very important to note that by using FE analysis similar to the previous section without considering a specified control volume, everybody can simply and conveniently evaluate the J-integral for any cracked members introduced in the FSWed CSCB specimens virtually made of the equivalent material.

According to J-integral criterion, failure occurs when the value of J-integral around the crack tip reaches the critical value of J-integral, called J_{Ic}. For plane stress, the following expression can be utilized for evaluating J_{Ic} [32]:

$$J_{Ic} = \frac{K_c^2}{E} \tag{7}$$

This equation can be directly utilized for EMC-based calculations. Thus, since the welded zone is assumed to be made of virtual brittle material, it is better that two important parameters mentioned above, namely the parameters J_k and J_{Ic} should be named as $J_{eq/EMC}$ and $J_{cr/EMC}$. By using Eq. (7), the value of parameter $J_{cr/EMC}$ for the welded zone for all of tested samples is found to be equal to 25.02 N/mm. As a consequence, to predict failure load of a CSCB specimen loaded under various mode mixities based on EMC-J criterion, the value of $J_{eq/EMC}$ should firstly be computed by an arbitrary load

(e.g. 1 N) by means of FE analysis. Then, the failure load is obtained when the value of $J_{eq/EMC}$ reaches $J_{cr/EMC}$. The values of the parameter $J_{eq/EMC}$ for all samples are presented in Table 5.

Table 5 Summary of the numerical results for determining the values of J and ASED for the tested FSWed CSCB specimens. The values of J and ASED in the table have been evaluated by applying a unit load in the FE numerical models.

β (deg.)	$ASED_{EMC}$ (MJ/m3)	$J_{eq/EMC}$ (N/mm)
0	3.29e-07	5.66e-07
25	1.89e-07	2.67e-07
45	6.04e-08	5.75e-08
56	2.40e-08	1.65e-08

4. Results and discussion

Mixed mode fracture behavior of the welded aluminum alloy specimens was evaluated by analyzing the CSCB specimens with pre-crack angles of β = 0◦, 25◦, 45◦, 56◦ by means of the ASED and J-integral approach. The results of the experimental and numerical analyses for pre-cracked specimens are presented in Table 6 and Fig. 7. In particular, Table 6 reports the experimental loads to failure, $P_{Exp.}$ for various mixed mode loading conditions compared with the theoretical values, $P_{EMC\text{-}ASED}$ and $P_{EMC\text{-}J}$ based on the ASED and J-integral evaluation. The relative discrepancy between the experimental failure loads of the CSCB specimens and the theoretical predictions obtained using ASED and J-integral criteria are presented in the last columns of Table 6 to evaluate the accuracy of the predictions using EMC-ASED and EMC-J approaches. As it can be observed from Table 6 and Fig. 8, the majority of failure load predictions are in good agreement with the experimental data with the average discrepancies of 10.0% and 12.2% for EMC-ASED and EMC-J criteria, respectively. According to the theoretical results, higher discrepancies were obtained for the specimens with pre-crack angles of 45 and 56 degree. Although the discrepancies are still in a good engineering range, two main reasons can be mentioned for such relatively high discrepancies. The first reason is the disability of EMC in

including the real size of the plastic zone around the crack at failure in computing the tensile strength of the equivalent material. As well established, the amount of plastic deformations around the crack tip (and hence, the strain energy required for crack extension) depends seriously on the mode mixity ratio. However, EMC does not deal with the plastic zone size and computes the tensile strength of the equivalent material by taking solely into account the tensile stress-strain curve of the ductile material. The second reason is, however, the local plastic deformations that form at the top loading point and the bottom supports (Fig. 3). These local plastic zones absorb some considerable energy and increase the failure loads. By increasing the contribution of mode II loading, the plastic zone size around the crack tip increases, leading to increasing the failure load. Trivially, a greater failure load results in greater local plastic regions at the top and bottom of the specimen, leading to larger energy dissipation.

Table 6 The experimental and theoretical critical loads for the tested FSWed CSCB specimens together with the discrepancies for EMC-ASED and EMC-J criteria.

β (deg.)	$P_{Exp.}$ (N)	$P_{EMC\text{-}ASED}$ (N)	Dis (%)	$P_{EMC\text{-}J}$ (N)	Dis (%)	Size of plastic zone (mm)
0	6915	6731	2.7	6646	3.9	1.7 (MSY)
25	9590	8872	7.5	9668	0.8	-----
45	17371	15705	9.6	20842	20.0	-----
56	31284	24904	20.4	38891	24.3	5 (LSY)
Average discrepancies			**10.0 %**		**12.2 %**	

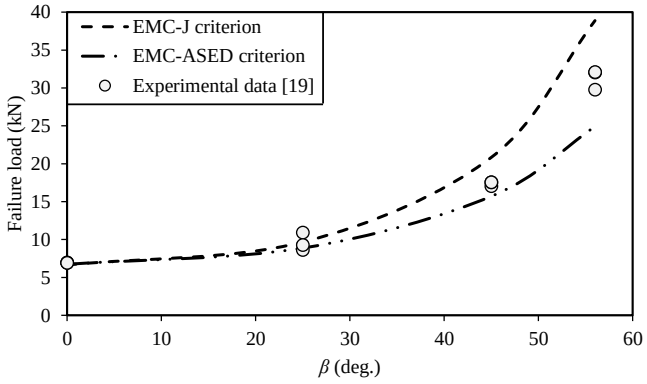

Fig. 7. Variations of failure load versus the crack inclination angle β for EMC-ASED and EMC-J criteria together with the experimental results of the CSCB FSWed specimens.

Fig. 8 presents a comprehensive synthesis expression of the square root of the average SED normalized by the critical SED obtained from EMC, $W_{cr/EMC}$ (which is proportional to the failure load), as a function of the pre-crack angle β. According to Fig. 8, it is verified that the size of control volumes and the critical SED value obtained using the EMC formulation is suitable to characterize the failure of the FSWed materials containing pre-cracks. Almost all of the theoretical predictions fall into a scatter band of ±25% with majority of them falling into a scatter band of ±10%. It is worth mentioning that the scatter band observed in this research is in an acceptable range compared to the results obtained in terms of ASED for other materials reported in the open literature [33-36]. Although the current research was conducted on FSWed Al 6061-T6 and Al 7075-T6 specimens, however, it is expected to get similar results for other aluminium alloys welded with the same technique.

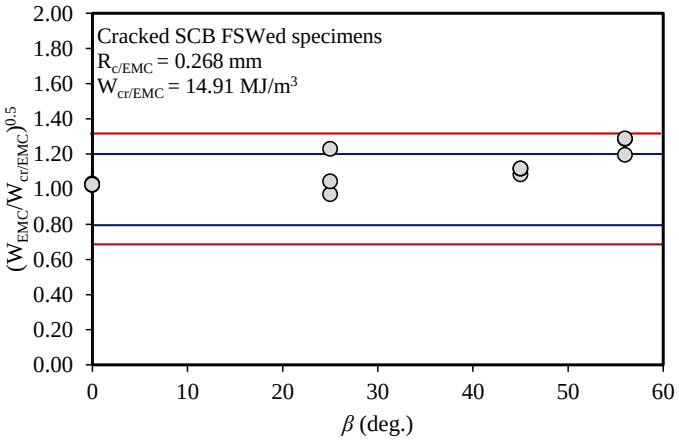

Fig. 8. Synthesis of failure loads in terms of normalized ASED.

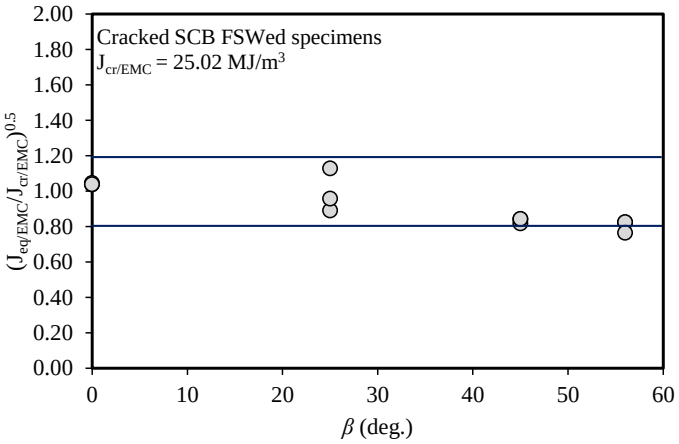

Fig. 9. Synthesis of failure loads in terms of normalized J-integral.

Considering the critical loads predicted by the two combined energy-based criteria i.e. EMC-ASED and EMC-J criteria are in good agreement with the experimental results (see Table 6). According to Table 6, the EMC-ASED results fall within the discrepancy band of ± 20.4% being most of them inside the band of 10%, whereas the EMC-J results had a discrepancy band of ± 24.3% being most of them inside the band of 20%. Hence, the theoretical results presented in this paper confirm that EMC-ASED criterion could be considered as a good choice for failure load prediction of FSWed CSCB specimens subjected to mixed mode I/II loading. It should be mentioned that the discrepancies reported in Table 6 were calculated using the mean value of experimental data for each case of loading.

As is evident in Table 6, higher accuracy of failure load prediction for the tested CSCB specimens can be obtained using the EMC-ASED criterion compared to EMC-J criterion. However, the performance of these two criteria for the case of LSY was almost the same. Both these criteria can be considered in the cases that engineering predictions with an acceptable precision and limited amount of numerical calculations are needed.

Although different accuracies were observed for the theoretical predictions based on these two energy-based failure criteria, each of them has its own special performance in prediction of onset of failure in

cracked components. Accordingly, both studied criteria can be frequently employed for failure prediction of different cracked components subjected to different loading conditions to discover their likely strong and weak points. Consequently, selecting any of the two energy-based models for failure assessment of FSWed cracked specimens does not necessarily mean that the other criterion should not be employed.

In point of fact, researchers in the field of structural integrity, designers and engineers should appropriately regulate which of the energy-based failure criteria can satisfy their favor for failure load estimation of ductile components with geometrical discontinuities. Put it differently, engineers should consider four essential characteristics namely the real-life application, the computational cost, the accuracy level, and the level of complexity to be able choose an appropriate ductile failure prediction model for their structural integrity analyses [37, 38].

5. Conclusions

Ductile failure of the FSWed Al 6061-T6 and Al 7075-T6 specimens under mixed mode loading conditions was investigated by equating the ductile behavior of the material with a virtual brittle material. Various pre-crack angles were considered for the FSWed CSCB specimens. Fracture tests were undertaken on CSCB specimens containing an inclined pre-crack. According to the experimental results, the FSWed cracked specimens under mode I and mixed mode I/II loading conditions failed by the moderate and large-scale yielding regimes, respectively. As an alternative way to evaluate the failure of welded material with substantial plastic deformation around the crack tip, the EMC was used to consider an equivalent brittle material for the tested specimens. The virtual ultimate strength resulted from EMC was then used in two linear elastic based fracture criteria namely ASED and J-integral to evaluate the ductile failure of the cracked specimens. Application of this methodology instead of

sophisticated elastic-plastic analyses results in a straightforward evaluation of failure in materials with considerable plastic deformation. In this way, the failure loads of the cracked welded specimens under mixed mode loading were successfully predicted by the two energy based criteria. Finally, it can be concluded that both criteria are superior and appropriate for designers who need relatively simple calculations with acceptable accuracies.

Funding sources

This research did not receive any specific grant from funding agencies in the public, commercial, or not-for-profit sectors.

References

[1] Kasman, Ş., Kahraman, F., 2014. Investigations for the effect of parameters on the weld performance of AA 5083-H111 joined by friction stir welding. Proc. Inst. Mech. Eng. B J. Eng. Manuf. 228, 937-946.

[2] Bahemmat, P., Besharati, M.K., Haghpanahi, M., Rahbari, A., Salekrostam, R., 2010. Mechanical, micro-, and macrostructural analysis of AA7075–T6 fabricated by friction stir butt welding with different rotational speeds and tool pin profiles. Proc. Inst. Mech. Eng. B J. Eng. Manuf. 224, 419-433.

[3] Leal, R.M., Chaparro, B.M., Antunes, J.M., Vilaça, P., Rodrigues, D.M., Loureiro, A., 2008. Mechanical behaviour of FSW aluminium tailored blanks. Mater Sci. Forum 587, 961-965.

[4] Peel, M., Steuwer, A., Preuss, M., Withers, P.J., 2003. Microstructure, mechanical properties and residual stresses as a function of welding speed in aluminium AA5083 friction stir welds. Acta mater. 51, 4791-4801.

[5] Guo, J.F., Chen, H.C., Sun, C.N., Bi, G., Sun, Z., Wei, J., 2014. Friction stir welding of dissimilar materials between AA6061 and AA7075 Al alloys effects of process parameters. Mater. Design, 56, 185-192.

[6] Palanivel, R., Mathews, P.K., Dinaharan, I., Murugan, N., 2014. Mechanical and metallurgical properties of dissimilar friction stir welded AA5083-H111 and AA6351-T6 aluminum alloys. Trans. Nonferrous Met. Soc. China 24, 58-65.

[7] Kundu, J., Singh, H., 2016. Friction stir welding of dissimilar Al alloys: effect of process parameters on mechanical properties. Eng. Solid Mech. 4, 125-132.

[8] Aliha, M.R.M., Shahheidari, M., Bisadi, M., Akbari, M., Hossain, S., 2016. Mechanical and metallurgical properties of dissimilar AA6061-T6 and AA7277-T6 joint made by FSW technique. Int. J. Adv. Manuf. Technol. 86, 2551-2565.

[9] Moreira, P., Jesus, A.M.P., Ribeiro, A.S., Castro, P., 2008. Fatigue crack growth behaviour of the Friction Stir Welded 6082-T6 aluminium alloy. Revista da Associação Portuguesa de Análise Experimental de Tensões ISSN. 1646, 70-78.

[10] Raghuram, V., 2009. Fatigue fracture and microstructural analysis of friction stir welded butt joints of aerospace aluminum alloys. Master's Theses, Louisiana State University, 1827.

[11] Mokhtar, S.N.F., Wahab, A.A., Karuppanan, S., 2012. Fracture Toughness and Fatigue Crack Growth Study of Friction Stir Welded Plates. J. Appl. Sci. 12, 2469-2473.

[12] Alavi Nia, A., Shirazi, A., 2018. An investigation into the effect of welding parameters on fatigue crack growth rate and fracture toughness in friction stir welded copper sheets. Proc. Inst. Mech. Eng. L J. Mater. Des. Appl. 232(3), 191-203.

[13] Ghahremani Moghadam, D., Farhangdoost, K., 2016. Influence of welding parameters on fracture toughness and fatigue crack growth rate in friction stir welded nugget of 2024-T351 aluminum alloy joints. Trans. Nonferrous Met. Soc. China 26, 2567-2585.

[14] Kulekci, M.K., Mendi, F., Sevim, I., Basturk, O., 2005. Fracture toughness of friction stir welded joints of AlCu4SiMg aluminium alloy. Metalurgija 44, 209-213.

[15] Seib, E., Koçak, M., Assler, H., 2004. Fracture assessment of welded aerospace aluminium alloys using SINTAP route. Weld. World 48, 2-8.

[16] Syafiq, W.M., Rojan, M.A., Majid, M.S.A., Jaafar, N.A., 2016. Fracture toughness of friction stir welded aluminum alloy. J. Eng. Appl. Sci. 11(5), 3571-3577.

[17] Aliha, M.R.M., Fotouhi, Y., Berto, F., 2018. Experimental notched fracture resistance study for the interface of Al–Cu bimetal joints welded by friction stir welding. Proc. Inst. Mech. Eng. B J. Eng. Manuf. 232(12), 2192-2200.

[18] Sutton, M.A., Reynolds, A.P., Yang, B., Taylor, R., 2003. Mixed mode I/II fracture of 2024-T3 friction stir welds. Eng. Fract. Mech. 70, 2215-2234.

[19] Torabi, A.R., Kalantari, M.H., Aliha, M.R.M., 2018. Fracture analysis of dissimilar Al-Al friction stir welded joints under tensile/shear loading. Fatigue Fract. Engng Mater. Struct. 41(9), 2040-2053.

[20] Torabi, A.R., Berto, F., Razavi, S.M.J., 2018. Tensile failure prediction of U-notched plates under moderate scale and large-scale yielding regimes. Theor. Appl. Fract. Mech. 97, 434-439.

[21] Torabi, A.R., Habibi, R., 2016. Investigation of ductile rupture in U-notched Al 6061-T6 plates under mixed mode loading. Fatigue Fract. Eng. Mater. Struct. 39(5), 551-565.

[22] Cicero, S., Torabi, A.R., Madrazo, V., Azizi, P., 2018. Prediction of fracture loads in PMMA U-notched specimens using the equivalent material concept and the theory of critical distances combined criterion. Fatigue Fract. Engng Mater. Struct. 41(3), 688-699.

[23] Majidi, H.R., Golmakani, M.E., Torabi, A.R., 2018. On combination of the equivalent material concept and J integral criterion for ductile failure prediction of U-notches subjected to tension. Fatigue Fract. Engng Mater. Struct. 41(7), 1476-1487.

[24] Torabi, A.R., 2012. Estimation of tensile load-bearing capacity of ductile metallic materials weakened by a V-notch: The equivalent material concept. Mater. Sci. Eng. A 536, 249-255.

[25] Torabi, A.R., Berto, F., Razavi, S.M.J., 2018. Ductile failure prediction of thin notched aluminum plates subjected to combined tension-shear loading. Theor. Appl. Fract. Mech. 97, 280-288.

[26] Lazzarin, P., Zambardi, R., 2001. A finite-volume-energy based approach to predict the static and fatigue behavior of components with sharp V-shaped notches. Int. J. Fract. 112, 275–298.

[27] Lazzarin, P., Berto, F., 2005. Some Expressions for the Strain Energy in a Finite Volume Surrounding the Root of Blunt V-notches. Int. J. Fract. 135(1-4), 161-185.

[28] Rice, J.R., 1968, A path independent integral and the approximate analysis of strain concentration by notches and cracks.ASME.

[29] Cherepanov, G., 1967. The propagation of cracks in a continuous medium. J. Appl. Math. Mech. 31, 503-512.

[30] Kim, Y., Shim, D., Choi, J., Kim, Y., 2002. Elastic plastic analyses for surface cracked plates under combined bending and tension. J. Strain Anal. Eng. Des. 37, 33-45.

[31] Chen, Y.H., Lu, T.J., 2004. On the path dependence of the J-integral in notch problems. Int. J. Solids Struct. 41, 607-618.

[32] Yoda, M., 1980. The J-integral fracture toughness for Mode II. Int. J. Fract. 16(4), R175–R178.

[33] Berto, F., Lazzarin, P., 2014. Recent developments in brittle and quasi-brittle failure assessment of engineering materials by means of local approaches. Mater. Sci. Eng. Reports 75, 1–48.

[34] Majidi, H.R., Ayatollahi, M.R., Torabi, A.R., Zaheri, A., 2018. Energy-based assessment of brittle fracture in VO-notched polymer specimens under combined compression-shear loading conditions. Int J Damage Mech Doi:http://doi.org/10.1177/1056789518780424.

[35] Aliha, M.R.M., Berto, F., Mousavi, A., Razavi, S.M.J., 2017. On the applicability of ASED criterion for predicting mixed mode I+II fracture toughness results of a rock material. Theor Appl Fract Mech 92, 198-204.

[36] Razavi, S.M.J., Aliha, M.R.M., Berto, F., 2018. On the applicability of ASED criterion for predicting mixed mode I+II fracture toughness results of a rock material. Theor Appl Fract Mech 97, 419-425.

[37] Majidi, H.R., Torabi, A.R., Golmakani, M.E., 2018. J-integral expression for mixed mode I/II ductile failure prediction of U-notched Al 6061–T6 plates under large-scale yielding regime. Eng Fract Mech 195, 253–66.

[38] Majidi, H.R., Razavi, S.M.J., Torabi, A.R., 2019. Application of EMC-J criterion to fracture prediction of U-notched polymeric specimens with nonlinear behaviour. Fatigue Fract Eng Mater Struct 42(1), 352–62.

Table captions

Table 1 Tensile properties of Al 7075-T6 and Al 6061-T6 for the FSW butt weld process (Torabi 2018a).

Table 2 Dimensions of CSCB sample.

Table 3 list of experimental failure loads for the whole CSCB samples.

Table 4 Mesh sensitivity analysis with different element sizes.

Table 5 Summary of the numerical results for determining the values of J and ASED for the tested FSWed CSCB specimens. The values of J and ASED in the table have been evaluated by applying a unit load in the FE numerical models.

Table 6 The experimental and theoretical critical loads for the tested FSWed CSCB specimens together with the discrepancies for EMC-ASED and EMC-J criteria.

Figure captions

Fig. 1 Schematic of CSCB specimen.

Fig. 2 A quality of the surface on a sample welded joint.

Fig. 3 Some of the CSCB samples.

Fig. 4 Typical load-displacement curve related to a specific CSCB sample (Torabi et al. 2018a).

Fig. 5. (a) Typical tensile stress-strain curve for a ductile material (b) SED absorbed by the equivalent material until final fracture.

Fig. 6. A mesh pattern for FSWed CSCB specimen under pure mode I loading.

Fig. 7. Variations of failure load versus the crack inclination angle β for EMC-ASED and EMC-J criteria together with the experimental results of the CSCB FSWed specimens.

Fig. 8. Synthesis of fracture data in terms of normalized ASED.

Fig. 9. Synthesis of fracture data in terms of normalized J-integral.